OsteoArthritis and Cartilage (2006) **14,** 906–913

doi:10.1016/j.joca.2006.03.001

Osteoarthritis and Cartilage

International Cartilage Repair Society

OARSI OSTEOARTHRITIS RESEARCH SOCIETY INTERNATIONAL

Lead accumulation in tidemark of articular cartilage

N. Zoeger Ph.D.†*, P. Roschger Ph.D.‡, J. G. Hofstaetter M.D.‡§, C. Jokubonis†, G. Pepponi Ph.D.‖, G. Falkenberg Ph.D.¶, P. Fratzl Ph.D.††, A. Berzlanovich M.D.‡‡§§, W. Osterode M.D., Ph.D.‖‖, C. Streli Ph.D.† and P. Wobrauschek Ph.D.†

† *Vienna University of Technology, Atominstitut, Stadionallee 2, 1020 Vienna, Austria*

‡ *Ludwig Boltzmann Institute of Osteology, Hanusch Hospital of WGKK and AUVA Trauma Centre Meidling, 4th Medical Department, Hanusch Hospital, Vienna, Austria*

§ *Department of Orthopaedics, Vienna General Hospital, Medical University of Vienna, A-1090 Vienna, Austria*

‖ *ITC-irst, Centro per la Ricerca Scientifica e Tecnologica, via Sommarive 18, 38050 Povo, Trento, Italy*

¶ *Hamburger Synchrotronstrahlungslabor HASYLAB am Deutschen Elektronen-Synchrotron, Notkestrasse 85, 22603 Hamburg, Germany*

†† *Max-Planck Institute of Colloids and Interfaces, Department of Biomaterials, Am Mühlenberg, D-14476 Potsdam-Golm, Germany*

‡‡ *Department of Forensic Medicine, Medical University of Vienna, A-1090 Vienna, Austria*

§§ *Department of Forensic Medicine, University of Munich, D-80377 Munich, Germany*

‖‖ *Universitätsklinik für Innere Medizin IV, Vienna General Hospital, Medical University of Vienna, A-1090 Vienna, Austria*

Summary

Objective: Determination of the spatial distribution of the toxic element lead (Pb) and other trace elements in normal articular cartilage and subchondral bone from adult humans with no history of work-related exposure to Pb.

Methods: Four macroscopically normal femoral heads and three patellas were harvested from randomly selected forensic autopsies. All subjects died of acute illnesses, had no history of work-related exposure to Pb and had no metabolic bone disease. The elemental distribution of lead (Pb) together with zinc (Zn), strontium (Sr) and calcium (Ca) in the chondral and subchondral region was detected using high resolution synchrotron radiation induced micro X-ray fluorescence (SR μ-XRF) analysis. SR μ-XRF line scans in conventional and SR μ-XRF area scans in confocal geometry were correlated to backscattered electron (BE) images visualizing the mineralized tissue.

Results: In all samples, we found a highly specific accumulation of Pb in the tidemark, the transition zone between calcified and non-calcified articular cartilage. Pb fluorescence intensities in the tidemark, which is thought to be a metabolically active mineralization front, were 13-fold higher when compared to subchondral bone. Pb intensities in the subchondral region were strongly correlated with Zn, but were distinctly different from Ca and Sr.

Conclusions: The finding of the highly specific accumulation of lead in the tidemark of human articular cartilage is novel. However at this point, the exact mechanisms of the local Pb accumulation as well as its clinical implications are unknown.

Key words: Lead accumulation, Tidemark, Synchrotron micro XRF, Calcified cartilage.

Introduction

One of the main threats to human health from heavy metals is associated with exposure to Pb. Exposure to Pb is associated with chronic diseases in the nervous, hematopoietic, skeletal, renal and endocrine systems[1]. Although much progress has been made to limit lead exposure in industrialized countries, primarily through the elimination of leaded gasoline, workplace exposures and leaded pipes, most adults have already accumulated a substantial body burden of Pb[2,3]. The half-life of Pb in the blood is 1 month, but it accumulates in the skeleton, where approximately 95% of the total body burden of Pb is present[4] with an estimated half-life up to 20 years[5]. Diseases or states with increased bone turnover, such as osteoporosis, pregnancy, hyperthyroidism and hyperparathyroidism are associated with increased mobilization of Pb from the skeleton[6–8]. Aging-associated release of bone lead into the circulation is a potentially important source of soft-tissue lead exposure and toxicity[9]. Moreover, reports in humans and animals support a role of Pb in osteopenia[9,10] and Carmouche *et al.* have recently shown in an experimental mouse model that exposure to lead inhibits fracture healing[11]. They were able to

*Address correspondence and reprint requests to: Dr Norbert Zoeger, Vienna University of Technology, Atominstitut, Stadionallee 2, A-1020 Vienna, Austria. Tel: 43-1-58801-14133; Fax: 43-1-58801-14199; E-mail: zoeger@ati.ac.at

Received 17 August 2005; revision accepted 5 March 2006.

show that Pb exposure leads to an increased cartilage formation with delayed maturation and calcification and increased formation of fibrous tissue during bone repair.

Moreover, intra-articular lead has shown to lead to osteoarthritic changes in the knee joint in humans[12] as well as in experimental animal models[13,14]. Osteoblasts and chondrocytes seem to be important target cells for the toxic effects of Pb[15], however, surprisingly little is known about how Pb is distributed in bone and cartilage at the microscopic level. Pb becomes incorporated into bone during mineralization[16] and remains there until bone is resorbed by osteoclasts[4]. Previous studies on the distribution of Pb in bone differentiated only between compact and trabecular bone and lacked any further spatial resolution[4,17,18]. To date, there are no data available on Pb distribution in the osteochondral unit of articular joints.

The osteochondral unit has a highly complex structure designed to enable friction free movements in articulating joints, to resist static and dynamic loads and to transfer loads from articular cartilage to the underlying bone. It is composed basically of articular cartilage forming superficial, transitional, deep and calcified zones with different fibril features and subchondral bone tissue[19]. The zone of calcified cartilage is about 100 μm thick and forms a tight bonding of cartilage to bone, two materials very different in stiffness[20]. Interestingly, the mineral particles impregnating the organic matrix in calcified articular cartilage are similar with that in bone[21], though its chemical composition is very different[19]. In general the mineralization density in calcified articular cartilage is higher than in bone, while surprisingly the stiffness of both calcified materials is comparable[20]. However, little is known about mechanisms and dynamics of the mineralization process in this region. The transition zone between calcified and non-calcified cartilaginous matrix, the so called tidemark, seems to be the metabolically active front of calcification[22].

The purpose of this study was to establish a spatially resolved distribution of Pb in the chondral and subchondral region from normal humans using synchrotron radiation induced micro X-ray fluorescence (SR μ-XRF) analysis. This technique enables non-destructive detection of Pb and other trace elements in the femtogram range at the micrometer level, which cannot be achieved by other micro analytical techniques (e.g., Electron Probe Micro Analysis, EPMA). Moreover, an inherent advantage of this method is its multielement detection capability, which enables to detect different elements simultaneously[23].

Methods

SAMPLES AND SAMPLE PREPARATION

Four femoral heads and three patellas were harvested from five (three females, two males) randomly selected forensic autopsies. All individuals died of illnesses of the heart and the great vessels or accidents and had no history of metabolic bone disease or Pb exposure. Furthermore, samples were selected on basis of having no macroscopical signs of osteoarthritis. In two cases, one femoral head and one patella were taken from the same individual. In two cases, one single femoral head and in one case, a single patella was harvested. The average age of the subjects was 57 years (ranging from 48 to 65). The study was approved by the Institutional Ethical Review Board of the Department of Forensic Medicine of the Medical University of Vienna.

Five-millimeter-thick sections were cut perpendicular to the articular surface from the central region of patella (sagittal plane) as well as from the superior, weight bearing region of the femoral head (frontal plane). Samples were fixed in 70% ethanol, dehydrated through a series of alcohol, and embedded in polymethylmethacrylate (PMMA)[24]. After trimming, surfaces of the PMMA-blocks were polished using diamond suspension and carbon coated for backscattered electron (BE) imaging. Afterwards, 200-μm-thick slices containing the bone area analyzed by BE imaging were cut using a low speed diamond saw (Buehler Isomed, Lake Pluff, USA) for SR μ-XRF analysis.

BE IMAGING

BE imaging is a validated technique to visualize and quantify calcium concentration distribution in bone and mineralized cartilage[20,21,25] and is based on the backscattering of electrons from the sample surface in a scanning electron microscope. A digital scanning electron microscope (DSM 962, Zeiss, Oberkochen, Germany) equipped with a four quadrant semiconductor BE-detector was employed. The microscope was operated at an acceleration voltage of 20 kV, the working distance kept at 15 mm, and the probe current was maintained at 110 pA. Images at a series of magnifications 12−500× were acquired. The intensity of the BE signal is proportional to the average atomic number of the target material. In case of bone the BE signal is dominated by its Ca content − the element with the highest atomic number ($Z = 20$). Thus, areas in the BE image with bright gray levels reflect mineralized matrix with high Ca contents, whereas areas with dark gray levels indicate low mineral density.

The BE images provide the spatial distribution of mineralization density at the sectioned tissue surface with an information depth about 1 μm. Areas of mineralized cartilage have a more homogenous intrinsic structure and have a higher degree of mineralization than bone. Cement-lines are transition zones between different bone packets and/or mineralized cartilage with a generally high mineral content and a homogenous intrinsic structure.

The tidemark is a typical narrow seam of gradually increasing mineral content at the border between non-calcified and calcified articular cartilage[20,21]. Younger bone packets have a characteristic lower mineral content (lower gray level in BE images) than older more mature bone packets[26].

SR μ-XRF ANALYSIS (LINE SCANS)

SR μ-XRF is a powerful analytical tool for qualitative and quantitative analysis of the chemical elements present in the sample[23], based on the detection of characteristic X-rays induced by high energy primary photons.

An inherent advantage of this method is its multielement detection capability, which enables the detection of different elements simultaneously[23].

The unique properties of synchrotron radiation, notably high photon flux, natural collimation, polarization and tunability of the energy of the primary photons, resulting in absolute detection limits on the femtogram level for medium Z elements, allow the analysis of trace elements in bone. The outstanding features of synchrotron radiation in combination with novel X-ray optics were exploited to investigate the elemental distribution in bone on a microscopic scale. SR μ-XRF measurements have been carried out at the micro focus end-station at HASYLAB, beamline L, Hamburg, Germany, by scanning the sample along a line in steps of

10 μm relative to an X-ray micro beam (beam cross section 13 μm). The primary X-ray beam was monochromatized at 18 keV by a Ni/C multilayer monochromator and focused by a polycapillary half lens onto the sample. At each point of the scan a fluorescence spectrum was recorded for 100 s by an energy dispersive lithium drifted silicon semiconductor detector (Gresham Sirius 80) providing information on the chemical elements present in the sample simultaneously. Using this setup, fluorescence intensities for lead (Pb), calcium (Ca), zinc (Zn) and strontium (Sr) were detected from the 200-μm-thick sample. Besides Pb and Ca data for Zn and Sr were also evaluated, since these are two elements known to be critical in bone metabolism and mineralization[27–30]. The element- and matrix-specific information depth for different characteristic X-rays ranged between 40 μm for Ca and 600 μm for Sr. Spectra were processed spectra using AXIL software from the QXAS package for peak deconvolution and subtraction of the radiation background. Subsequently, plotting the obtained intensities vs the relative sample position gives the distribution of each element along the line scan. In order to visualize simultaneously the distribution of Ca, showing high intensities, and the trace elements with low intensities, the intensity curve for each element has been normalized to its maximum value. In total, 11 scans across articular cartilage and subchondral bone were performed on four samples of femoral head and three patellas (Table I). To correlate the distribution of chemical elements with micro structural features of bone, we overlaid data obtained from SR μ-XRF line scans with BE images defining the tidemark, as well as the interface between calcified cartilage and subchondral bone. In order to quantify spatial variations in Pb and Zn intensities within the sample, baseline intensities were defined. Since the intensities in the subchondral region showed low variation in signal, Pb and Zn intensities in this region were averaged and used as baselines. The subchondral region was defined by BE imaging. Paired *t*-test (two tailed) was used to evaluate statistical significance between areas of different Pb and Zn intensities compared to baseline (Graph Pad Prism 4.0). Statistical significance was set at the 95% confidence limit. Since Ca and Sr showed a relative homogeneous distribution across the scans, no rationing was applied to this data.

Table I
Relative Pb and Zn intensities in the transition zone (tz) between non-calcified and calcified articular cartilage of femoral head (FH) and patella (P) normalized to baseline intensities in subchondral bone (sub)

Sample, Scan	Pb(tz)/Pb(sub)	Zn(tz)/Zn(sub)
FH1,a*	12.3	4.3
FH2,a**	10.5	2.6
FH2,b**	10.1	3.6
FH3,a	14.9	3.9
FH4,a	9.7	3.5
FH4,b	18.0	3.9
P1,a*	9.1	2.5
P1,b*	14.1	3.7
P2,a**	16.1	1.8
P2,b**	17.3	2.2
P3,a	11.2	3.0
Average ratio	13 ± 3.2#	3.2 ± 0.8##

Intensity ratios for each scan as well as the average ratio for all scans are given. Paired samples are marked with * and **, respectively. # Indicates $P < 0.005$; ## indicates $P < 0.001$.

CONFOCAL SR μ-XRF ANALYSIS (AREA SCANS)

SR μ-XRF in confocal geometry[31] with an additional polycapillary half lens in front of the detector was used for depth defined area scans and three-dimensional (3D)-reconstructions. By overlapping the focal spots of the two X-ray optics a well defined micro-volume is achieved from which the fluorescence radiation is detected. The size of the detection volume at an energy of 9.7 keV (Au-Lα photons) was measured to be of $22 \times 14 \times 20$ μm^3 (lateral × height × depth) by scanning a 4-μm-thick Gold (Au) foil and a 4-μm-thick Tungsten (W) wire through the beam. The method was used to detect fluorescence signals from the surface layer as well as from subsurface layers of about 20 μm in thickness. Due to the second capillary optics the detectors field of view is restricted to the orbital plane of the synchrotron storage ring, which allows an optimal use of the linear polarization of the synchrotron radiation. Therefore, the radiation background in the fluorescence spectra is reduced and the measuring time per pixel can be reduced. In a typical area scan fluorescence spectra at 41×41 pixels (400×400 μm^2) with a measuring time of 5 s/pixel have been recorded and afterwards processed as described above. Elemental maps from fluorescence data were generated by a custom made software and matched with BE images.

Furthermore, a 3D reconstruction of elemental intensity maps obtained by confocal SR μ-XRF of a sample volume of $200 \times 200 \times 160$ μm^3 was performed on a patella slice. The voxel size was $10 \times 10 \times 10$ μm^3 and data acquisition time for each voxel was 5 s. X-ray fluorescence spectra were recorded on a 3D grid of 7497 ($21 \times 21 \times 17$, width × height × depth) measurement points. The net intensities for each element were determined from the fluorescence spectra by automatic peak fitting (AXIL) and were converted to 8-bit grayscale images for each measured slice in depth. From these images element-specific 3D volumes were rendered using a visualization software, designed for tomographic imaging.

Results

SR μ-XRF LINE SCANS IN NON-CONFOCAL GEOMETRY

Firstly, SR μ-XRF line scans in non-confocal (conventional) geometry were performed across articular cartilage and subchondral bone in each sample. A representative line scan with a corresponding BE image from the subchondral region of the femoral head [Fig. 1(a and b)] is shown in Fig. 1(c).

In the zone of non-calcified cartilage, no characteristic X-ray intensities of Ca, Zn, Sr, and Pb were detected.

In the transition zone between non-calcified and calcified articular cartilage a marked increase in signal of all the elements was observed. In contrast to Ca and Sr, the Pb and Zn signals exhibited a peak distinctly before Ca and Sr reached a plateau coinciding with the region of calcified cartilage as indicated by BE image. Pb intensities rapidly declined within the first 100 μm of calcified cartilage and remained relatively constant and low in subchondral bone. When compared to subchondral bone baseline intensities we found a 13-fold increase ($P < 0.005$) of Pb intensities in the transition zone between non-calcified and calcified articular cartilage. Zn intensities also rapidly declined within the first 100 μm of calcified cartilage, but remained at a relatively higher baseline level than Pb. When compared to subchondral bone baseline intensities we found a 3.2-fold increase in Zn intensity ($P < 0.001$) in the transition zone. These findings for Pb

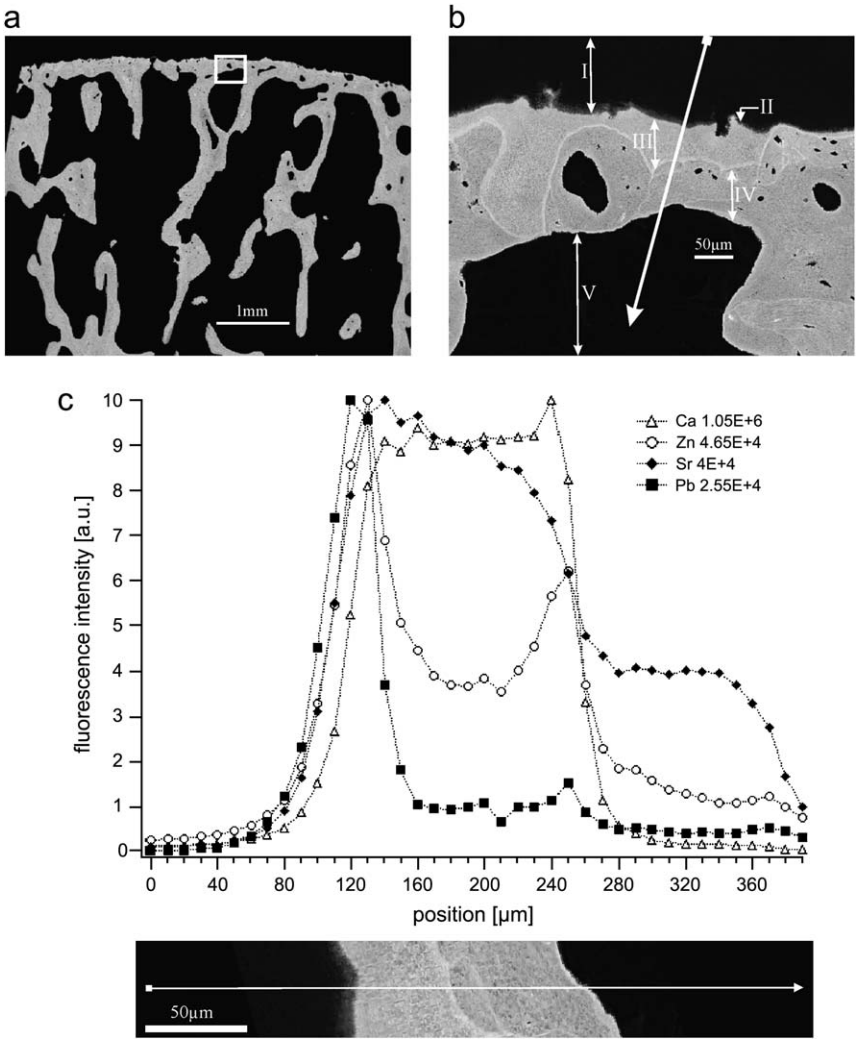

Fig. 1. (a) BE image of an analyzed 200-μm section of femoral head visualizing the mineralized areas of the sample. (b) Magnified image of the framed box. An SR μ-XRF scan (arrow) performed across (I) non-calcified articular cartilage, (II) the transition zone between non-calcified and calcified articular cartilage, (III) calcified articular cartilage, (IV) subchondral bone and the (V) marrow cavity. (c) Striking Pb and Zn maxima were seen in the transition zone between non-calcified and calcified articular cartilage. Maximum fluorescence intensities were normalized to 10 (absolute values for each element are given in the box). Due to differences in information depths for characteristic X-rays and irregular sample shape, an exact local correlation among intensity profiles and BE image is not possible.

and Zn were highly consistent and were observed for all scans on paired (femoral head and patella from one subject) as well as single autopsies (Table I).

In the zone of subchondral bone, intensity levels of the elements were relatively constant. No Ca and Pb signals were detected in the bone marrow cavity as defined by the BE image. Interestingly, at the border between subchondral bone and the marrow cavity Zn signal levels first increased and then dropped down to low levels in the marrow cavity. Sr signals were also detected in the bone marrow region.

SR μ-XRF AREA SCAN IN CONFOCAL GEOMETRY

Secondly, a confocal SR μ-XRF area scan was performed to obtain the distribution of Ca, Zn, Sr and Pb at the surface of a patella sample. Comparison of elemental maps [Fig. 2(b)] with the corresponding BE image of the scanned region revealed that none of the investigated elements were present in the zone of non-calcified articular cartilage. The intensity map for Pb showed strikingly increased fluorescence intensities in the transition zone between non-calcified and calcified cartilage, known as the tidemark[22]. Except small elevations in cement-lines, Pb intensities were relatively constant and low in calcified cartilage and subchondral bone. A similar distribution was detected for Zn, where we also found increased intensities in both the tidemark and the cement-lines. In contrast to Pb and Zn, Ca and Sr showed a very homogeneous distribution in calcified cartilage and subchondral bone. However, Sr signals appeared to be relatively more decreased than Ca signals in areas of less calcified bone matrix [dark gray levels in Fig. 2(a)].

More quantitative conclusions could be drawn from fluorescence intensity profiles [Fig. 2(c)] which have been extracted from the elemental maps along the marked line in Fig. 2(b). Strikingly, Pb and Zn intensities were dramatically increased in the tidemark region and were almost back to

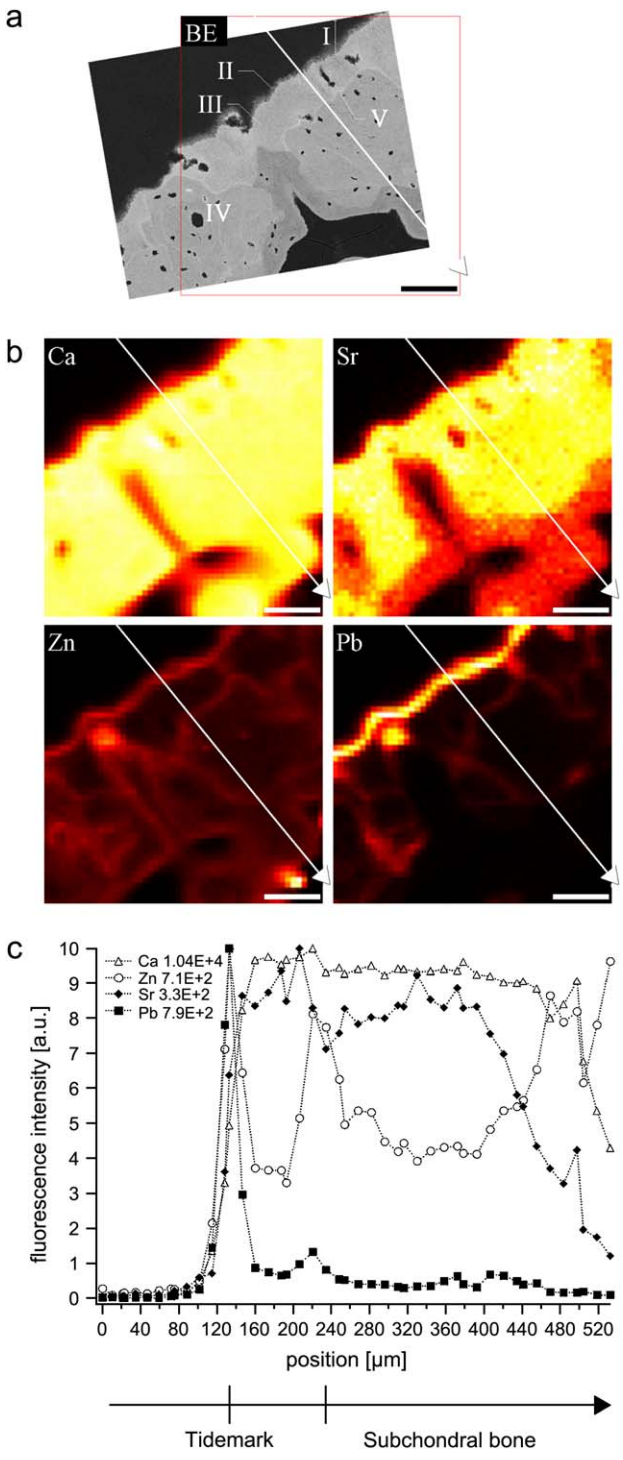

Fig. 2. (a) BE image of analyzed chondral/subchondral region of the patella. Non-calcified cartilage (I), tidemark (II), calcified cartilage (III), subchondral bone (IV), and cement-lines (V) can be clearly identified. Length of scale bar corresponds to 100 µm. (b) Ca, Zn, Sr, Pb signal intensity maps of the corresponding region. (c) Fluorescence intensity profiles along the marked line. Maximum fluorescence intensities were normalized to 10 (absolute values for each element are given in the box). Pb and Zn maxima could be exactly allocated to the tidemark of articular cartilage.

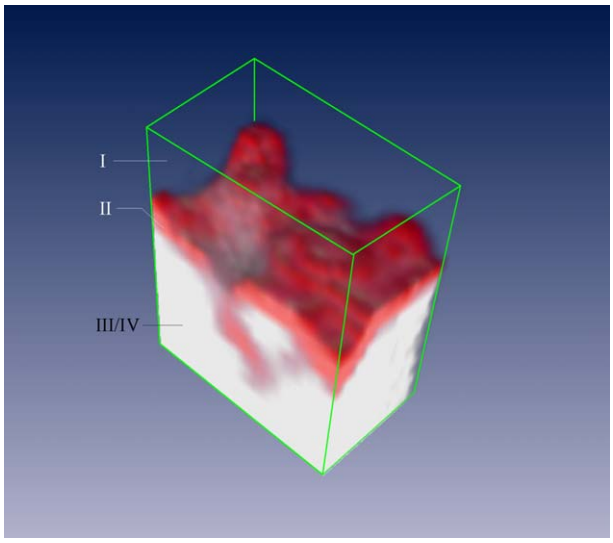

Fig. 3. Pb intensity maps (red) of a chondral/subchondral region of the patella in a sample volume of 200 × 200 × 160 µm^3. The calcified tissue (coherently scattered signal) is visualized as white. (I) Non-calcified articular cartilage, (II) transition zone (tidemark), (III) calcified articular cartilage and (IV) subchondral bone.

baseline intensities before Ca intensity levels reached the maximum level. We found distinct changes in the Pb/Ca and the Zn/Ca ratios between the tidemark (50/1000 and 90/1000, respectively) and subchondral bone (1/1000 and 22/1000, respectively). Pb intensities at the cement-lines were about 10% of the Pb intensities at the tidemark, whereas Zn intensities at the cement-lines were about 80–90% when compared to the tidemark. Interestingly, although intensity maxima of Pb and Zn coincided in the tidemark, considerable differences of intensity profiles were found in the subchondral bone. When compared to Pb levels, we found a smaller relative decrease in Zn signal in subchondral bone as well as a greater relative increase in cement-lines.

Furthermore, a 3D reconstruction of the Pb distribution was generated from confocal SR µ-XRF area scans performed in different depth on a patella sample (Fig. 3). The results of the 3D renderings are in accordance with two-dimensional (2D) data sets as well as line scans obtained by SR µ-XRF in non-focal geometry. Furthermore, the 3D feature of Pb accumulation in the tidemark indicates that this accumulation of Pb is not limited to surface area of the sample, but is also present in the deeper regions of the sample.

Discussion

In this study we established spatially resolved elemental profiles and maps of Ca, Sr, Zn and Pb in articular cartilage and subchondral bone of femoral head and patella from healthy adult humans and correlated them to BE images. Our data clearly show that the toxic trace element Pb is accumulated very specifically in the transition zone between the non-calcified and the calcified articular cartilage known as the tidemark[22].

SR µ-XRF was shown to be an excellent technique to determine simultaneously the spatial distribution of various elements like Ca, Sr, Zn, Pb in human bone samples with

high sensitivity. The use of high flux, monochromatic and linear polarized synchrotron radiation enables to determine traces of Pb in matrices containing elements with low and medium atomic numbers. The spatial resolution of the method is limited by the minimum beam size achievable by X-ray optics being used (about 13 μm in the present study). When performing SR μ-XRF analyses in non-confocal (conventional) geometry on samples thicker than the beam sizes a degradation in the lateral resolution is observed. Due to element- and matrix-specific information depths for different characteristic X-rays, effects of tissue geometry do not allow always an exact local correlation among Ca, Sr, Zn and Pb intensity profiles as well as a precise assignment to the BE images[32]. Thus, the different information depth for BE imaging (1 μm) and XRF also may explain the fact that Zn and Sr intensities were detected in the marrow cavity, where no bone material was present on the BE image. However, confocal SR μ-XRF analysis of the 200-μm-thick bone slices helped to eliminate the unwanted contribution of deeper sample layers to the X-ray fluorescence spectra. Therefore, the overall spatial resolution of the system was improved by an order of magnitude from 200 μm to 20 μm. Using the confocal setup it was assured that the detected characteristic X-rays for each element originated from the same sample depth. Therefore, the matching of BE images and element maps was facilitated. Furthermore, confocal SR μ-XRF enabled for a 3D reconstruction of the Pb distribution in various depths of the articular cartilage and subchondral bone sample. Thus, for the first time a visualization of the 3D nature of the Pb accumulation in the tidemark (Fig. 3) could be achieved.

The tidemark has been thought of as a metabolically active calcification front advancing in the direction of the non-calcified cartilage. Duplication of the tidemark, which can be observed in osteoarthritis[33], is seen as evidence for this advancement. The tidemark can be labeled with tetracycline[22] and can be stained by dyes that stain basophilic substance and lipids[34], or by enzymes such as ATPase and alkaline phosphatase[35]. The high specificity and reproducibility of Pb accumulation in adult articular cartilage led us to believe that this could be a general phenomenon. Interestingly, our results indicate that Zn, an essential element for normal growth of the skeleton[28,36], is also accumulated in the tidemark as well as in cement-lines and at sites of new bone formation. This result is in accordance with that of Gomez *et al.*[27], who have shown previously that the highest concentrations of Zn in bone were found at sites of new bone formation.

Regarding the possible biological role of Pb, it has a higher affinity than calcium to osteocalcin, increases the amount of mineral bound to osteocalcin[37,38] and has shown to interfere with Ca^{2+} signaling in cells by competing for calcium binding sites[39]. Moreover, Pb is able to displace Ca^{2+} by cation exchange processes in the hydroxyapatite crystal[40], which could alter the hydroxyapatite crystal and thus affect its material properties. To date, very little data are available on how Pb affects bone material properties and bone crystal structure *in vivo*. However at this point, one can only speculate about the exact mechanisms of Pb accumulation in the tidemark of articular cartilage. Moreover, the tidemark has also great clinical importance, because it is the region of critical mechanical weakness in articular cartilage[41] where clefts may open due to injuries and osteoarthritis[42].

Although local Pb has been shown to lead to osteoarthritis[12–14] and the fact that osteoblasts and chondrocytes seem to be important target cells for the toxic effects of Pb[15], there is very limited knowledge on the molecular mechanisms of Pb toxicity in these tissues. There are no data available whether systemic exposure to the toxic heavy metal Pb affects the risk of developing osteoarthritis. Osteoarthritis, the clinical syndrome of joint pain and dysfunction caused by joint degeneration, affects more people than any other joint disease. The incidence of osteoarthritis rises precipitously with age; as a result, the prevalence and burden of this disorder is increasing rapidly[43]. The increased remodeling found in the subchondral bone in osteoarthritis may play an important role in its disease progress[44]. Moreover, this increased resorption of subchondral bone during osteoarthritis[45,46] could also cause an increased release of Pb into the circulation as seen in osteoporosis[8] and hyperthyroidism[6].

Tibia and patella have been widely used in epidemiologic studies to determine bone Pb levels by *in-vivo* K-lines XRF. Interestingly, with this technique the patella was found to contain more Pb per bone weight than compact bone of the tibia[8]. However, due to the large information depth ($\geq$2 cm) when considering Pb K-lines (75 keV photons) in *in-vivo* XRF analysis, signals are not only detected from the trabecular region of the patella, but also from the articular cartilage of the patella and even from the distal femur. Our findings may explain in part the higher Pb content found in the patella when compared to tibia using *in-vivo* K-line XRF.

In conclusion our findings of the specific accumulation of Pb in the tidemark of normal human adult articular cartilage may lead to further understanding and research on the effects of Pb on cartilage, bone biology and biomineralization.

Acknowledgments

The authors would like to thank Dr Dariusz Wegrzynek (IAEA Seibersdorf Laboratories, XRF Instrumentation Group) for the help with the three-dimensional visualization of the data.
This work was supported by the Austrian Science Fund (FWF), project number P15740 and the European Commission, project number I-01038EC.

References

1. Jarup L. Hazards of heavy metal contamination. Br Med Bull 2003;68:167–82.
2. Pirkle JL, Brody DJ, Gunter EW, Kramer RA, Paschal DC, Flegal KM, *et al*. The decline in blood lead levels in the United States. The National Health and Nutrition Examination Surveys (NHANES). JAMA 1994;272(4):284–91.
3. Vig EK, Hu H. Lead toxicity in older adults. J Am Geriatr Soc 2000;48(11):1501–6.
4. Wittmers LE Jr, Aufderheide AC, Wallgren J, Rapp G Jr, Alich A. Lead in bone. IV. Distribution of lead in the human skeleton. Arch Environ Health 1988;43(6): 381–91.
5. Rabinowitz MB. Toxicokinetics of bone lead. Environ Health Perspect 1991;91:33–7.
6. Osterode W, Reining G, Manner G, Jager J, Vierhapper H. Increased lead excretion correlates with desoxypyridinoline crosslinks in hyperthyroid patients. Thyroid 2000;10(2):161–4.
7. Osterode W, Winker R, Bieglmayer C, Vierhapper H. Effects of parathyroidectomy on lead mobilization from bone in patients with primary hyperparathyroidism. Bone 2004;35(4):942–7.

8. Tsaih SW, Korrick S, Schwartz J, Lee ML, Amarasiriwardena C, Aro A, *et al*. Influence of bone resorption on the mobilization of lead from bone among middle-aged and elderly men: the Normative Aging Study. Environ Health Perspect 2001;109(10): 995–9.
9. Silbergeld EK, Schwartz J, Mahaffey K. Lead and osteoporosis: mobilization of lead from bone in postmenopausal women. Environ Res 1988;47(1): 79–94.
10. Escribano A, Revilla M, Hernandez ER, Seco C, Gonzalez-Riola J, Villa LF, *et al*. Effect of lead on bone development and bone mass: a morphometric, densitometric, and histomorphometric study in growing rats. Calcif Tissue Int 1997;60(2):200–3.
11. Carmouche JJ, Puzas JE, Zhang X, Tiyapatanaputi P, Cory-Slechta DA, Gelein R, *et al*. Lead exposure inhibits fracture healing and is associated with increased chondrogenesis, delay in cartilage mineralization, and a decrease in osteoprogenitor frequency. Environ Health Perspect 2005;113(6):749–55.
12. Slavin RE, Swedo J, Cartwright JJ, Viegas S, Custer EM. Lead arthritis and lead poisoning following bullet wounds: a clinicopathologic, ultrastructural, and microanalytic study of two cases. Hum Pathol 1988; 19(2):223–35.
13. Harding NR, Lipton JF, Vigorita VJ, Bryk E. Experimental lead arthropathy: an animal model. J Trauma 1999; 47(5):951–5.
14. Bolanos AA, Vigorita VJ, Meyerson RI, D'Ambrosio FG, Bryk E. Intra-articular histopathologic changes secondary to local lead intoxication in rabbit knee joints. J Trauma 1995;38(4):668–71.
15. Puzas JE, Sickel MJ, Felter ME. Osteoblasts and chondrocytes are important target cells for the toxic effects of lead. Neurotoxicology 1992;13(4):783–8.
16. Flood PR, Schmidt PF, Wesenberg GR, Gadeholt H. The distribution of lead in human hemopoietic tissue and spongy bone after lead poisoning and Ca-EDTA chelation therapy. Observations made by atomic absorption spectroscopy, laser microbeam mass analysis and electron microbeam X-ray analysis. Arch Toxicol 1988;62(4):295–300.
17. Han S, Li W, Jamil U, Dargan K, Orefice M, Kemp FW, *et al*. Effects of weight loss and exercise on the distribution of lead and essential trace elements in rats with prior lead exposure. Environ Health Perspect 1999; 107(8):657–62.
18. Aro A, Amarasiriwardena C, Lee ML, Kim R, Hu H. Validation of K x-ray fluorescence bone lead measurements by inductively coupled plasma mass spectrometry in cadaver legs. Med Phys 2000;27(1):119–23.
19. Wong M, Carter DR. Articular cartilage functional histomorphology and mechanobiology: a research perspective. Bone 2003;33(1):1–13.
20. Gupta HS, Schratter S, Tesch W, Roschger P, Berzlanovich A, Schoeberl T, *et al*. Two different correlations between nanoindentation modulus and mineral content in the bone–cartilage interface. J Struct Biol 2005;149(2):138–48.
21. Zizak I, Roschger P, Paris O, Misof BM, Berzlanovich A, Bernstorff S, *et al*. Characteristics of mineral particles in the human bone/cartilage interface. J Struct Biol 2003;141(3):208–17.
22. Lemperg R. The subchondral bone plate of the femoral head in adult rabbits. I. Spontaneus remodelling studied by microradiography and tetracycline labelling. Virchows Arch A Pathol Pathol Anat 1971;352(1): 1–13.
23. Van Grieken R, Markowicz A. Handbook of X-Ray Spectrometry. New York/Basel: Marcel Dekker Inc. 2002.
24. Roschger P, Plenk H Jr, Klaushofer K, Eschberger J. A new scanning electron microscopy approach to the quantification of bone mineral distribution: backscattered electron image grey-levels correlated to calcium K alpha-line intensities. Scanning Microsc 1995;9(1): 75–86.
25. Roschger P, Fratzl P, Eschberger J, Klaushofer K. Validation of quantitative backscattered electron imaging for the measurement of mineral density distribution in human bone biopsies. Bone 1998;23(4):319–26.
26. Misof BM, Roschger P, Cosman F, Kurland ES, Tesch W, Messmer P, *et al*. Effects of intermittent parathyroid hormone administration on bone mineralization density in iliac crest biopsies from patients with osteoporosis: a paired study before and after treatment. J Clin Endocrinol Metab 2003;88(3): 1150–6.
27. Gomez S, Rizzo R, Pozzi-Mucelli M, Bonucci E, Vittur F. Zinc mapping in bone tissues by histochemistry and synchrotron radiation-induced X-ray emission: correlation with the distribution of alkaline phosphatase. Bone 1999;25(1):33–8.
28. Calhoun NR, Smith JCJ, Becker KL. The role of zinc in bone metabolism. Clin Orthop 1974;103:212–34.
29. Grynpas MD, Marie PJ. Effects of low doses of strontium on bone quality and quantity in rats. Bone 1990; 11(5):313–9.
30. Oliver WR. X-ray fluorescence analysis of strontium in bone. Lab Pract 1968;17(6):690–718.
31. Janssens K, Proost K, Falkenberg G. Confocal microscopic X-ray fluorescence at the HASYLAB microfocus beamline: characteristics and possibilities. Spectrochim Acta B 2004;59(10–11):1637–45.
32. Zoeger N, Wobrauschek P, Streli C, Pepponi G, Roschger P, Falkenberg G, *et al*. Distribution of Pb and Zn in slices of human bone by synchrotron μ-XRF. X-Ray Spectrom 2005;34(2):140–3.
33. Lane LB, Bullough PG. Age-related changes in the thickness of the calcified zone and the number of tidemarks in adult human articular cartilage. J Bone Joint Surg Br 1980;62(3):372–5.
34. Boskez AL, Bullough PG, Dmitrovsky E. The biochemistry of the mineralizing front. Metab Bone Dis Relat Res 1980;2(S):61–7.
35. Dimitrovsky E, Lane LB, Bullough PG. The characterization of the tidemark in human articular cartilage. Metab Bone Dis Relat Res 1978;1:115–36.
36. Nishi Y. Zinc and growth. J Am Coll Nutr 1996;15(4): 340–4.
37. Dowd TL, Rosen JF, Mints L, Gundberg CM. The effect of Pb(2+) on the structure and hydroxyapatite binding properties of osteocalcin. Biochim Biophys Acta 2001; 1535(2):153–63.
38. Dowd TL, Rosen JF, Gundberg CM, Gupta RK. The displacement of calcium from osteocalcin at submicromolar concentrations of free lead. Biochim Biophys Acta 1994;1226(2):131–7.
39. Pounds JG, Long GJ, Rosen JF. Cellular and molecular toxicity of lead in bone. Environ Health Perspect 1991; 91:17–32.
40. Mavropoulos E, Rossi AM, Costa AM, Perez CA, Moreira JC, Saldanha M. Studies on the mechanisms

of lead immobilization by hydroxyapatite. Environ Sci Technol 2002;36(7):1625–9.
41. Kumar P, Oka M, Nakamura T, Yamamuro T, Delecrin J. Mechanical strength of osteochondral junction. Nippon Seikeigeka Gakkai Zasshi 1991;65(11): 1070–7.
42. Landells JW. The reactions of injured human articular cartilage. J Bone Joint Surg Br 1957;39-B(3):548–62.
43. Buckwalter JA, Saltzman C, Brown T. The impact of osteoarthritis: implications for research. Clin Orthop 2004;427 Suppl:S6–15.
44. Hayami T, Pickarski M, Zhuo Y, Wesolowski GA, Rodan GA, Duong LT. Characterization of articular cartilage and subchondral bone changes in the rat anterior cruciate ligament transection and meniscectomized models of osteoarthritis. Bone 2005.
45. Hayami T, Pickarski M, Wesolowski GA, McLane J, Bone A, Destefano J, *et al*. The role of subchondral bone remodeling in osteoarthritis: reduction of cartilage degeneration and prevention of osteophyte formation by alendronate in the rat anterior cruciate ligament transection model. Arthritis Rheum 2004; 50(4):1193–206.
46. Huebner JL, Hanes MA, Beekman B, TeKoppele JM, Kraus VB. A comparative analysis of bone and cartilage metabolism in two strains of guinea-pig with varying degrees of naturally occurring osteoarthritis. Osteoarthritis Cartilage 2002;10(10):758–67.